ARTICLES

Helical Superstructures of Fullerene Peapods and Empty Single-Walled Carbon Nanotubes Formed in Water

Naotoshi Nakashima,*,† Yasuhiko Tanaka,‡ Yasuhiko Tomonari,‡ Hiroto Murakami,‡ Hiromichi Kataura,§ Takahiro Sakaue,|| and Kenichi Yoshikawa||

Department of Chemistry and Biochemistry, Graduate School of Engineering, Kyushu University, Fukuoka 812-8581, Japan, Department of Science and Technology, Graduate School of Materials Science, Nagasaki University, Nagasaki 852-8521, Japan, Nanotechnology Research Institute, National Institute of Advanced Industrial Science and Technology, Central 4, Higashi 1-1-1, Tsukuba, Ibaraki, Japan, and Department of Physics, Graduate School of Science, Kyoto University, Kyoto 606-8502, Japan

Received: February 24, 2005; In Final Form: April 23, 2005

Aqueous dispersions of fullerene C_{70}-filled carbon nanotubes (C_{70}@SWNTs or peapods) and empty single-walled carbon nanotubes (empty SWNTs) were prepared with the aid of trimethyl-(2-oxo-2-pyrene-1-yl-ethyl)-ammonium bromide (**1**), which is a carbon nanotube solubilizer. This is the first report describing the preparation and characterization of the transparent dispersion/dissolution of the peapods. The UV−vis−near-IR spectra of C_{70}@SWNTs−**1** and empty SWNTs−**1** were almost identical. We found by means of transmission electron microscopy and atomic force microscopy that the empty SWNTs and C_{70}-peapods form helical nanostructures in the shapes of rings, irregular rings, lassos, handcuffs, catenanes, pseudorotaxanes, and figure-eight structures. The mechanism of the superstructure formation has been discussed in relation to the unique characteristics of stiff polymer chains with the aid of an off-lattice Monte Carlo simulation.

Introduction

Since their discovery in 1991,[1] carbon nanotubes have attracted much attention in various fields of nanoscience and nanotechnology due to their unique structural and electronic properties.[2−5] Fullerene-filled carbon nanotubes (so-called peapods) that were discovered by Luzzi et al.[6] in 1998 possess one-dimensional super-nanostructures and have been studied extensively.[7] Recently, considerable attention has focused on soluble carbon nanotubes via chemical modification and physical adsorption.[8−21] We have reported that polycyclic amphiphiles,[22] porphyrins,[23] and double-helical DNA[24] can solubilize single-walled carbon nanotubes (SWNTs) in aqueous or organic solutions (for details, see recent review article[12]).

The construction of nanoscaled superstructures via self-assembly or self-organization of carbon nanotubes is a great challenge, and soluble carbon nanotubes are good materials for the goal. In this paper, we focus on the formation of the superstructures of carbon nanotubes such as helices and rings via self-assembly in aqueous solutions. Avouris et al.[25] described the formation of the rings of SWNTs due to sonication from dispersed solutions in concentrated sulfuric acid and hydrogen peroxides. They suggested a nanotube ring-formation mechanism that involves the hydrophobic nanotubes acting as nucleation sites for bubble formation during sonication and that the ring formation is a kinetically controlled process where bubble cavitation provides the energy necessary to activate the ring formation. A theoretical approach to the formation of kinks, rings, and a "racket" structure of carbon nanotubes was described by Cohen et al.[26] Bertsche et al.[27] observed a ring of SWNTs with ultrahigh-vacuum scanning tunneling microscopy and spectroscopy. Sano et al.[28] described the ring closure of carbon nanotubes in an organic solution in the presence of dicyclohexylcarbodiimide. The electron transport, electrical switching, and rectification behaviors of the SWNT ring have been reported by Avouris et al.,[29] Watanabe et al.,[30] and Cuniberti et al.,[31] respectively. Terranova et al.[32] described that the synthesis of organized networks of helically wound SWNTs is possible. It is known that multiwalled carbon nanotubes (MWNTs) grow into a helically coiled structure under some experimental conditions.[33,34] Ahlskog et al.[35] described the ring formation of MWNTs in 2-propanol by sonication.

We now present the discovery that aqueous dispersions of empty SWNTs and of fullerene peapods prepared by using a carbon nanotube solubilizer trimethyl-(2-oxo-2-pyrene-1-yl-ethyl)-ammonium bromide (**1**)[22] form helical carbon nanotube

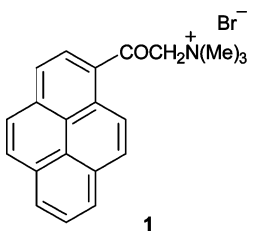

1

* Author to whom correspondence should be addressed. E-mail: nakashima-tcm@mbox.nc.kyushu-u.ac.jp.
† Kyushu University.
‡ Nagasaki University.
§ National Institute of Advanced Industrial Science and Technology.
|| Kyoto University.

10.1021/jp050958m CCC: $30.25
Published on Web 06/18/2005

superstructures in the shapes of rings, irregular rings, lassos, handcuffs, catenanes, and pseudorotaxanes. We have performed a numerical simulation by adopting an off-lattice Monte Carlo method with a Metropolis algorithm to gain insight into the mechanism of the helical superstructure formation.

Experimental Section

Materials. The empty SWNTs were synthesized by the laser furnace technique.[36] The preparation of fullerene C_{70}-peapods (C_{70}@SWNTs), which are more stable than the C_{60}-peapods and therefore easy to handle, has been described elsewhere.[36] The estimated filling rate of C_{70} was found to be higher than 70% by high-resolution transmission electron microscopy (HR-TEM) observations (Supporting Information, Figure S1). The average diameter of the C_{70}@SWNTs estimated by HRTEM and Raman scattering was 1.39 nm. We also used the so-called HiPco SWNTs (as-produced and purified, average diameter ca. 1 nm) that were purchased from the Carbon Nanotechnologies Co.

Trimethyl-(2-oxo-2-pyrene-1-yl-ethyl)-ammonium Bromide (1). An excess amount of trimethylamine gas was introduced to 1-(bromoacetyl)pyrene (191 mg, 0.59 mmol) in dry tetrahydrofuran (THF; 15 mL) at room temperature. This solution was then stirred for 1 day. The produced precipitate was separated and then dried in vacuo to give **1** as a yellow solid. Yield: 196 mg (87%). ^{1}H NMR (300 MHz, CD_3OD, 25 °C, TMS): δ = 8.1−9.1 (m, 9H, PyH), 4.1 (s, 2H, CH_2N^+), 3.6 (s, 9H, $(CH_3)_3N^+$). IR (KBr): ν = 3045 and 3012 cm^{-1} (ν_{C-H}, Ar), 1674 cm^{-1} ($\nu_{C=O}$). Elemental analysis; calcd (%) for $C_{21}H_{20}NOBr + 1.2H_2O$: C, 62.45; H, 5.59; N, 3.47. Found (%): C, 62.16; H, 5.21; N, 3.06.

Preparation of Aqueous Dispersions of Nanotubes. About 0.2 mg of the empty SWNTs (or C_{70}@SWNTs) and **1** in deuterium water (or Millipore water) was sonicated using a bath-type ultrasonic cleaner (Branson, model 5510) for 12 h, followed by centrifugation (8000*g*) of the suspension for 1 h to remove the insoluble nanotubes or peapods.

Characterization. The UV−vis−near-IR spectra were measured at 20 ± 1 °C using a spectrophotometer (JASCO, V-570). Transmission electron microscopy measurements were performed using a JEOL JEM-100S electron microscope. TEM samples were prepared by dipping a carbon-coated grid (Ouken-Shoji, 200-Å mesh) in the dispersion for 2−3 s, followed by air-drying. Atomic force microscopy (AFM) images were recorded on a SPI3800N (Seiko Instruments, Inc.) with a Si_3N_4 cantilever (SN-AF01). A freshly cleaved mica substrate was dipped into the dispersion and then dried in a vacuum to prepare the AFM sample.

Method of Simulation. To gain insight on the mechanism of the superstructure formation, we have performed numerical simulation.[37−40]

We adapted an off-lattice Monte Carlo simulation with a Metropolis algorithm on a single stiff polymer chain in three-dimensional (3D) space, where the polymer is described as a sequence of N = 500 spherical monomers with diameter σ connected by elastic bonds. The connectivity of the chain is maintained by the bonding energy between the neighboring monomers, modeled as a harmonic spring with cutoffs

$$U_{bond} = a(l - \sigma)^2 \quad \text{for } l_{min} < l < l_{max}$$

$$U_{bond} = \infty \quad \text{for } l \le l_{min} \text{ or } l \ge l_{max}$$

where we set $a = 20k_BT$, $l_{min} = 0.85\sigma$, and $l_{max} = 1.15\sigma$, respectively (k_B is the Boltzmann constant). The physicochemical property of the chain itself and the solution environment are specified by the additional two energetic terms, U_{bend} and U_{int}. The chain stiffness U_{bend} is introduced by the following bending potential.

$$U_{bend} = \kappa(1 - \cos\theta)^2$$

where κ is a parameter for the chain rigidity. To determine the general trend in stiff chains, we have performed the simulation by changing the stiffness parameter $\kappa = 500k_BT$ to $2000k_BT$. In the following, we exemplify the cases with $\kappa = 500k_BT$ and $1000k_BT$, corresponding to the persistence lengths of ca. 87σ and 135σ, respectively. The interaction between chain segments U_{int} is modeled by the Lennard-Jones potential.

$$U_{LJ} = 4\epsilon\left[\left(\frac{\sigma}{r}\right)^{12} - \left(\frac{\sigma}{r}\right)^{6} - c\right] \quad \text{for } r \le R_c$$

$$U_{LJ} = 0 \quad \text{for } r \ge R_c$$

where ϵ controls the strength of the interaction and $c = (\sigma/R_c)^{12} - (\sigma/R_c)^6$ so as to set the potential value to become zero at the cutoff $R_c = 2.5\sigma$. We investigated the cases with $\epsilon = 4k_BT$ and $8k_BT$. Both of these values on the monomer−monomer attractive interaction are found to be strong enough to stabilize the superstructures as exemplified in Figures 8 and 9.

From the randomly coiled initial conditions, the chain evolves its configuration through fluctuation. N trials of the elementary motion are defined as one Monte Carlo step.

Figure 1. Photo of aqueous solutions of (a) **1** (1 mM) and (b) C_{70}@SWNTs−**1** (**1** = 1 mM).

Results and Discussion

Spectral Features. We have previously described that **1** dissolves/disperses HiPco SWNTs in water and suggested the importance of π-stacking of the pyrene moiety with the sidewall of the nanotubes.[22] It was found that **1** can disperse both C_{70}@SWNTs and empty SWNTs in water (or deuterium water). Both obtained solutions were a transparent light black color. A typical photo is shown in Figure 1. Here again, the driving force of the dispersion/dissolution would be the $\pi-\pi$ interactions between the pyrene moieties on **1** with the sidewall of the peapods and empty nanotubes with diameter larger than the HiPco SWNTs. The absorption maxima of the UV−vis spectra of the C_{70}@SWNTs−**1** and of the empty SWNTs−**1** appeared at the same wavelengths, 232, 286, and 368 nm, together with a shoulder at 400 nm, which were almost identical with that of **1** only in water (Figure 2, left panel). Almost no spectral shift suggests that weak interactions between the pyrene moieties and the sidewall of the peapods and empty nanotubes or the

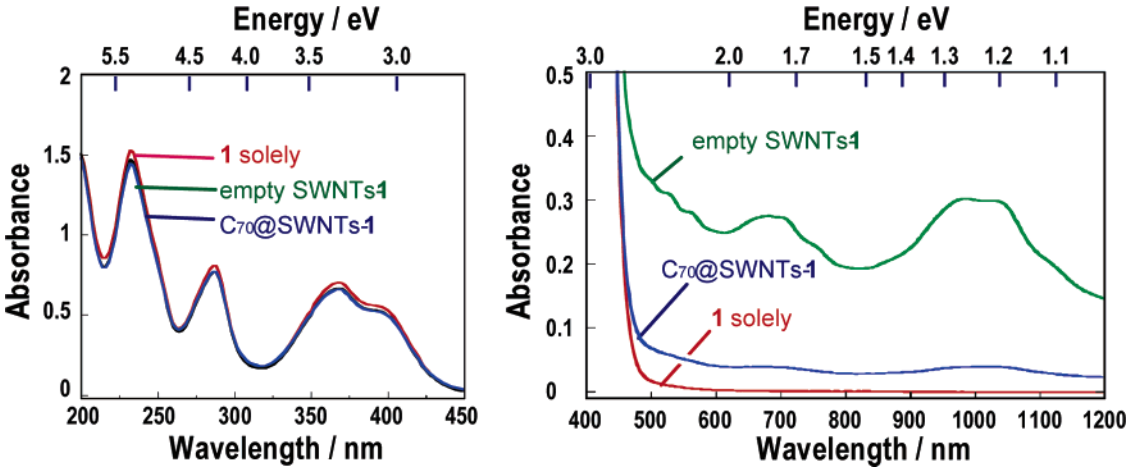

Figure 2. UV−vis−near-IR spectra of an aqueous solution of **1** (1 mM) and of aqueous dispersions of the empty SWNTs−**1** (**1** = 1 mM) and C_{70}@SWNTs−**1** (**1** = 1 mM). Optical cell length: left panel, 0.5 mm and right panel, 10 mm.

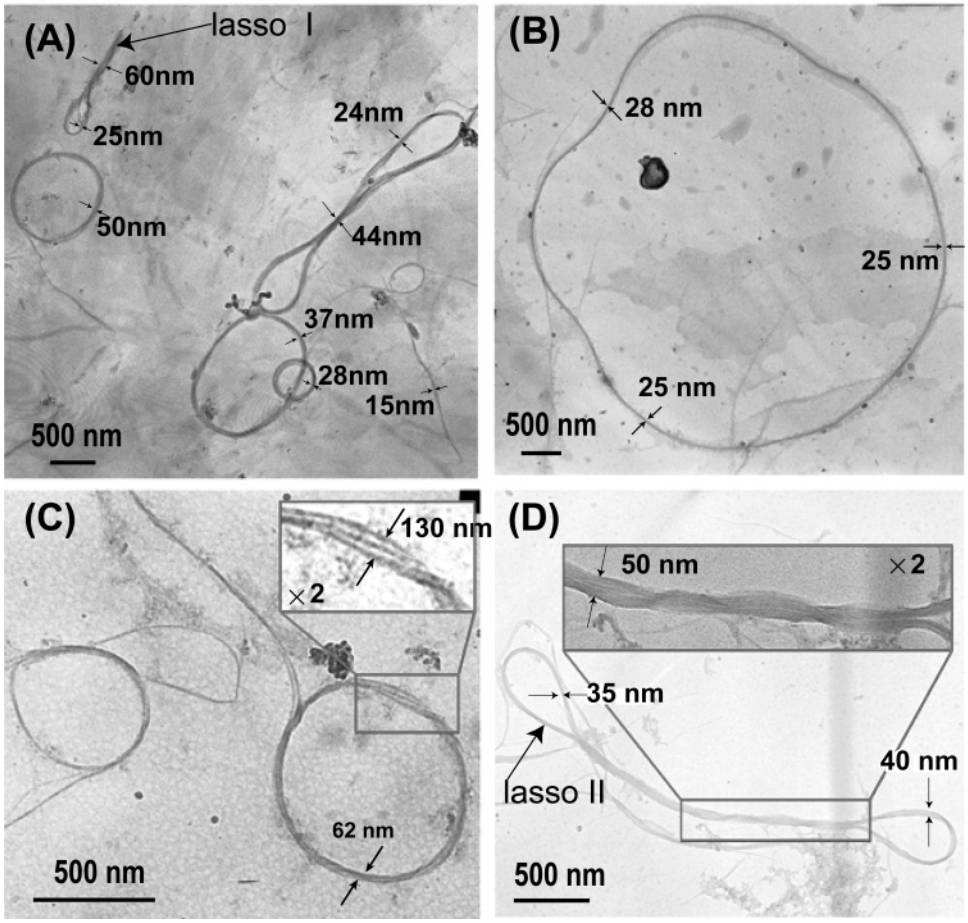

Figure 3. Typical TEM images of an aqueous dispersion of the C_{70}@SWNTs−**1** (**1** = 1 mM).

absorption spectra come from **1** in the bulk solution, not from **1** bound to the sidewall. The absorption of C_{70} encapsulated in the single-walled carbon nanotubes is not evident as is the case of the ethanol dispersion of the C_{70}@SWNTs.[41]

The near-IR peaks for both the C_{70}@SWNTs and empty SWNTs in the solutions appeared around 1000 and 680 nm (both broad, Figure 2, right panel). The former can be assigned to band-gap transitions in the second pair of singularities (S2) in the density of states of the semiconducting SWNTs, and the latter absorption is assigned to the first metallic (M1) band. Since the average diameter of the nanotubes is 1.39 nm, the observed absorption wavelength regions are almost identical with the theoretical band area[42] (for S2 and M1, 1040 and 690 nm, respectively). As can be seen in Figure 2, the metallic and semiconducting peaks of the C_{70}@SWNTs and empty SWNTs are very broad. This spectral feature is quite different from those of an aqueous solution of the as-produced and purified HiPco SWNTS in which sharp bands are seen (data not shown) like the individually dissolved HiPco SWNTs in aqueous solution of sodium dodecyl sulfate.[43] These results suggest that bundled C_{70}@SWNTs and empty SWNTs are formed in water. The aqueous solution of the C_{70}@SWNTs−**1** was further sonicated with a cup−horn-type ultrasonic homogenizer (SMT Co. UH-300) for 2 h to examine whether individual dissolution of the C_{70}@SWNTs occurs. We measured the vis−near-IR spectrum of the dispersion right after the sonication; however, the obtained

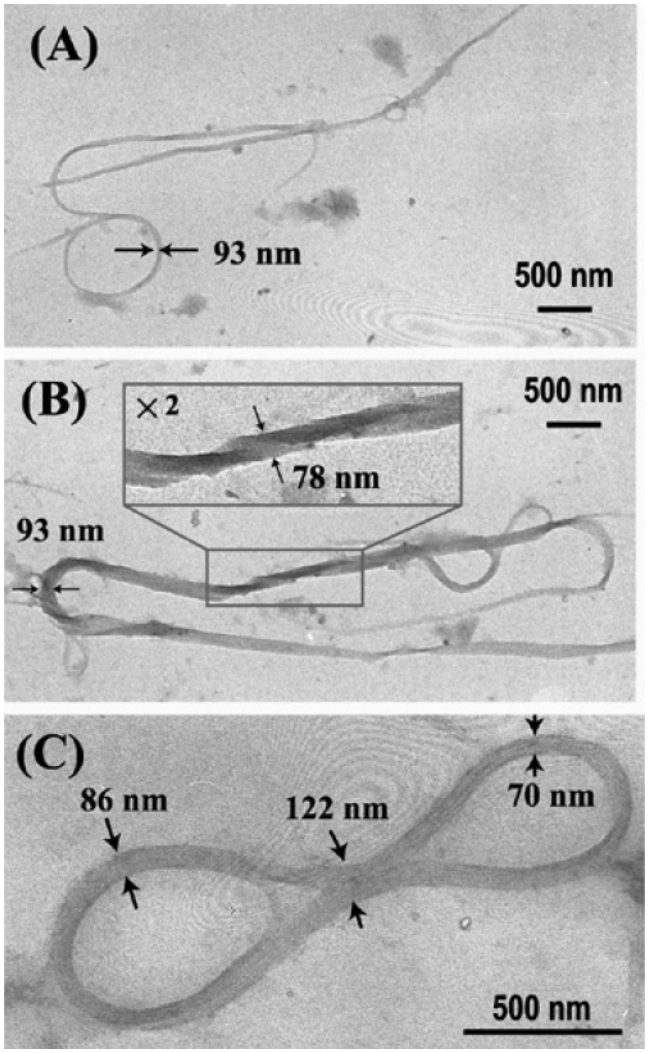

Figure 4. Typical TEM images of an aqueous dispersion of the empty SWNTs−**1** (**1** = 1 mM).

spectrum (data not shown) was the same as Figure 2 (right panel), suggesting that under these experimental conditions bundled peapods exist in the dispersed solution. However, we *unexpectedly* discovered helical superstructures of C_{70}@SWNTs in the dispersion, as described in the following section.

Helical Superstructure Formation. Figures 3 and 4 show typical TEM images of the aqueous dispersions of the C_{70}@SWNTs−**1** and empty SWNTs−**1**, respectively. In these figures, we see highly interesting topological images; that is, the peapods form rings with diameters of approximately 430, 870, and 1100 nm (Figure 3A), a lasso (lasso I in Figure 3A, length = ca. 1200 nm, ring diameter = ca. 250 nm), a catenane-like structure (Figure 3A, ring diameters = ca. 430 and 1100 nm), "handcuffs" (Figure 3A, length = ca. 3000 nm), an irregular ring (Figure 3B, diameter = ca. 6000 nm), another lasso (Figure 3C), and a lasso with double rings (lasso II in Figure 3D, length = ca. 3000 nm). As can be seen in Figure 4, the empty SWNTs−**1** also form superstructures including a lasso (Figure 4A) and a figure-eight shape with a size of 1800 nm × 600 nm (Figure 4C). The approximate probability of finding of such superstructures is about 10% of all the TEM images. The diameters of the rings of the SWNTs reported in the literature[25−28] are 600−800 nm. In this study, the diameters of the smaller rings are comparable to these reported values. However, in our case, we see very large rings; especially, the size of the irregular ring is much larger than that of the regular ring. These larger

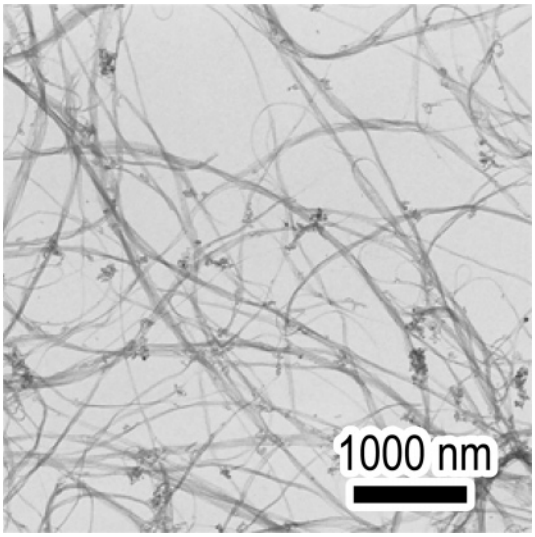

Figure 5. Typical TEM image of an ethanolic dispersion of the C_{70}@SWNTs−**1** (**1** = 1 mM).

rings would be expected to be flexible and may change their structures into lassos or the figure-eight shape.

More interestingly, we can clearly see the helix structure of the peapods and empty SWNTs in Figures 3C and 3D and Figure 4B. It is suggested that such topological superstructures would be formed from aggregation processes via a van der Waals interaction between the peapods (empty SWNTs) dispersed/dissolved in water using the solubilizer **1**.

Since both the C_{70}@SWNTs only and empty SWNTs only do not disperse in water, we obtained TEMs for the ethanolic dispersions of each single component of the C_{70}@SWNTs and empty SWNTs prepared by the sonication, and no such topological superstructure was observed in the dispersions (Figure 5). We have also used as-produced and purified HiPco SWNTs in place of the C_{70}@SWNTs and empty SWNTs and found no such superstructure is produced. These results suggest that the larger diameter size of the nanotubes that have stronger internanotube interactions is essential for the formation of the helical superstructures.

We now highlight the 3D structure of the aggregates by analyzing the AFM images of the C_{70}@SWNTs and empty SWNTs in water. A collection of the aqueous dispersions of the C_{70}@SWNTs−**1** and empty SWNTs−**1** together with their height profiles are presented in Figures 6 and 7, in which we can see a ring with the pseudorotaxane structure (Figure 6A), lassos (Figures 6B and 7A), a figure-eight shape (Figures 6C and 7B), and a helix with an unfolded structure together with a leaf shape (Figure 6D). Some of these AFM images are very similar to the TEM images shown in Figures 3 and 4. As shown in Figures 6 and 7, the *height profiles of the AFM images display the shapes of "mountain chains"*, which strongly indicate the formation of helical structures. The heights of many helical nanotubes are in the range of 5−15 nm.

The mechanism for the formation of the helical nanotubes (peapods) and the topological superstructures based on the helix can be deduced. The helix structure is one of the most stable structures formed via strong interactions between long strings. In this study, strong van der Waals interactions between several or more nanotube strings solubilized in water would be a driving force for the formation of the helical aggregated structures. The nanotubes with the larger diameters would be required to form such helical superstructures in water using the solubilizer. The regular and irregular rings of the peapods and empty nano-

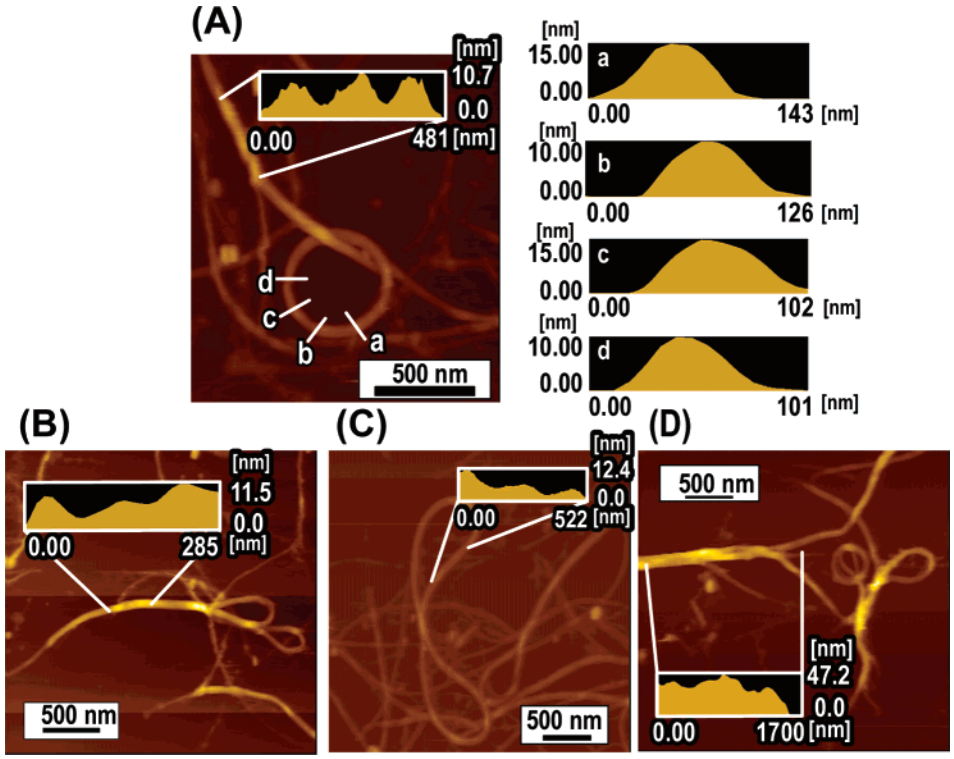

Figure 6. Typical AFM images of an aqueous dispersion of the C_{70}@SWNTs−**1** (**1** = 1 mM) and their height profiles.

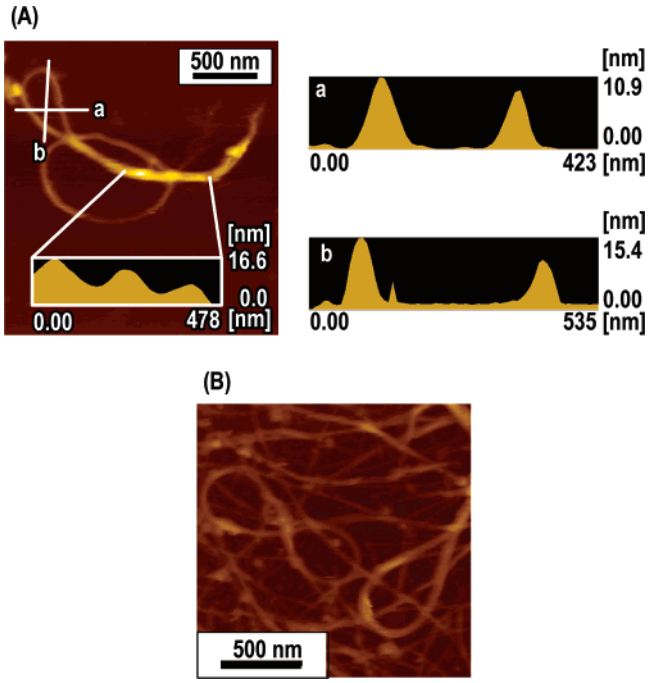

Figure 7. Typical AFM images of an aqueous dispersion of the empty SWNTs−**1** (**1** = 1 mM) and their height profiles.

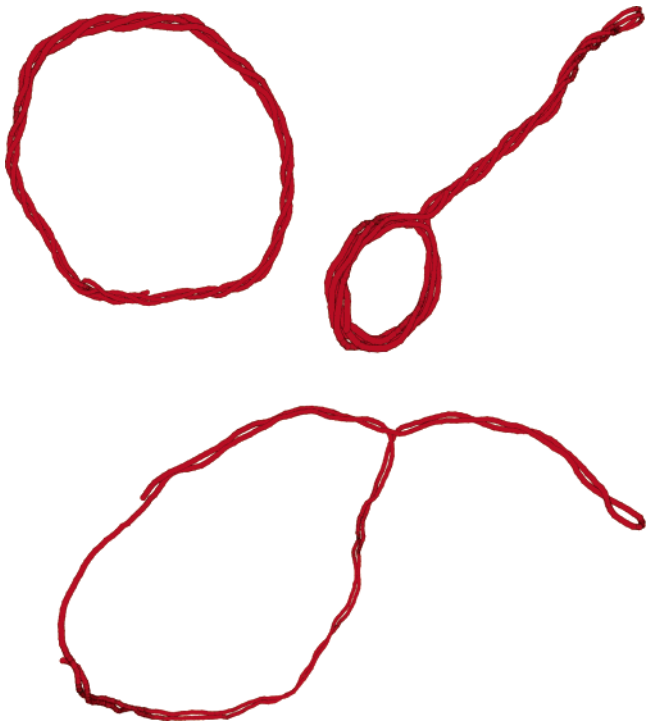

Figure 8. Examples of superstructures generated from single stiff polymer chains, obtained in Monte Carlo simulations. Parameters are $\kappa = 1000k_BT$ and $\epsilon = 8k_BT$ for the ring (top, left) and $\kappa = 500k_BT$ and $\epsilon = 4k_BT$ for the lasso (top, right) and the large lasso (bottom), respectively. These conformations are "frozen", exhibiting no significant morphological change under "thermal" fluctuation.

tubes would be formed by the same mechanism as for the SWNTs presented by Avouris and co-workers.[25] Twisting the ring followed by adhesion at the center might produce the figure-eight shape. The detailed mechanism for the formation of lassos and other superstructures is presented in the following section.

Results of Simulation. To shed light on the mechanism of superstructure formation from carbon nanotubes, we performed a Monte Carlo simulation on single stiff chains. As exemplified in Figure 8, a variety of folded morphologies have been observed in the simulation. Figure 9 shows the "time-dependent change" on the conformational change of a single stiff linear polymer. From the crossing at a point, the chain gradually shrinks accompanied by the formation of a stranded structure through the twisting of double or triple chains. Finally, tennis racket, or lasso-like, morphology is generated and keeps this shape as a stationary state. Besides such a conformational example, we

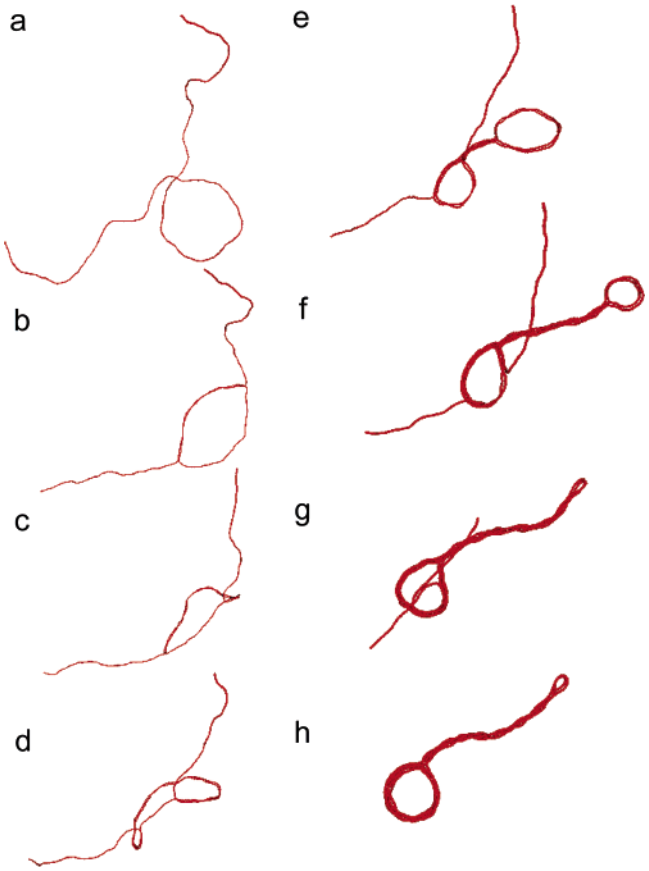

Figure 9. Conformational evolution of a single stiff polymer chain at $\kappa = 500k_BT$ and $\epsilon = 4k_BT$. The Monte Carlo steps are $s =$ (a) 0, (b) 50, (c) 100, (d) 150, (e) 200 (magnification, ×1.5), (f) 213 (magnification, ×2), (g) 230 (magnification, ×2), and (h) 250 (magnification, ×2), which are denoted by s in units of 10^4 Monte Carlo steps. The top (right) conformation in Figure 8 is the structure obtained after larger steps, $s = 500$, in the simulation given.

found that a variety of folded morphologies are generated in the simulation, such as rings, deformed rings, and rods. Here, it is noted that the stranded structure is spontaneously formed on a long stiff chain. In the following, we would like to discuss briefly the mechanism of formation of the stranded structure from an achiral polymer.

There are two competing factors in the shrinking process. One is strong attractive interaction between monomers, which prefer the collapsed structures, and the other is the high rigidity of the chain favoring the stretched conformations. As a consequence of the competition, the expected final structures are rings and/or rods from the equilibrium points of view.[37] However, due to the strong attractive interaction, which is necessary to collapse very stiff chains, the system is easily trapped in a nonoptimum, but metastable, conformation with respect to the free energy. The formation of the stranded structure found in the simulation products is also attributed to a kind of kinetic effect. During the "thermal" fluctuation of the conformation, a double and/or triple stranded stem is formed spontaneously in some region along the chain, while other parts of the chain form rings. These rings shrink with time by zipping, where this process is relatively slow. We expect that such slow conformational evolutions are rather common on the stiff chains. Therefore, if the chain adsorbs on the solid surface during this process, then we expect that kinetically frozen morphologies as shown in the present simulations may acquire further stability on the solid surface in actual experiments.

Aside from the morphological points of view, another specific feature on the collapsed products in the simulation is noted. It is found that all the collapsed products exhibit the dense packing with a few strands, which wind to form a helical structure. Indeed, we have performed simulations over a wide range of the parameter space and confirmed that stiff chains always form the helical structure mutually interwound by several strands upon the increase of the attraction between the polymer chains. As our model chain as well as carbon nanotube does not exhibit any chirality, the winding direction is spontaneously selected during the thermal fluctuation on the folding process, resulting in the chiral symmetry breaking on the helix.[39] It is generally expected that stiff polymer chains exhibit the ability to form helical structures as well as bundles.[40]

Conclusions

The polycyclic aromatic SWNT solubilizer **1** was found to disperse both C_{70}@SWNTs and empty SWNTs in water (or deuterium water). To our knowledge, this is the first example of the preparation of a dispersion/solution for fullerene peapods. TEM and AFM measurements revealed that both the peapods and empty SWNTs in the solutions form helical superstructures containing rings, lassos, catenanes, figure-eight shapes, and so forth. The scenario to produce such unique morphologies has been clarified by adopting an off-lattice Monte Carlo simulation. It might be possible, soon, to prepare these unique superstructures selectively from carbon nanotubes, as well as from other stiff polymers, by choosing suitable experimental conditions, through computer-aided design.

Acknowledgment. This study was supported, in part, by Grants-in-Aid from the Ministry of Education, Science, Sports, Culture and Technology, Japan. We thank Mr. Y. Misaki of Tokyo Metropolitan University for the HRTEM measurement of the peapods.

Supporting Information Available: HRTEM image of the peapods. This material is available free of charge via the Internet at http://pubs.acs.org.

References and Notes

(1) Iijima, S. *Nature* **1991**, *354*, 56.
(2) Harris, P. J. F. *Carbon Nanotubes and Related Structures*; Cambridge University Press: Cambridge, U. K., 1999.
(3) *The Science and Technology of Carbon Nanotubes*; Tanaka, K., Yamabe, T., Fukui, K., Eds.; Elsevier: Oxford, U. K., 1999.
(4) *Carbon Nanotubes: Synthesis, Structure, Properties and Applications*; Avouris, Ph., Dresselhaus, G., Dresselhaus M. S., Eds.; Spriger-Verlag: Berlin, Germany, 2001.
(5) Reich, S.; Thomsen, C.; Maultzch, J. *Carbon Nanotubes: Basic Concepts and Physical Properties*; Wiley-VCH: Berlin, Germany, 2004.
(6) Smith, B. W.; Monthioux, M.; Luzzi, D. E. *Nature* **1998**, *396*, 323.
(7) Khlobystov, A. N.; Britz, D. A.; Ardavan, A.; Briggs, G. A. D. *Phys. Rev. Lett.* **2004**, *92*, 245507 and references therein.
(8) Hirsch, A. *Angew. Chem., Int. Ed.* **2002**, *41*, 1853.
(9) Khabashesku, V. N.; Billups, W. E.; Margrave, J. L. *Acc. Chem. Res.* **2002**, *35*, 1087.
(10) Sun, Y.-P.; Fu, K.; Lin, Y.; Huang, W. *Acc. Chem. Res.* **2002**, *35*, 1096.
(11) Niyogi, S.; Hamon, M. A.; Hu, H.; Zhao, B.; Bhowmik, P.; Sen, R.; Itkis, M. E.; Haddon, R. C. *Acc. Chem. Res.* **2002**, *35*, 1105.
(12) Nakashima, N. *Int. J. Nanosci.* **2005**, *4*, 119.
(13) Chen, J.; Hamon, M. A.; Hu, H.; Chen, Y.; Rao, A. M.; Eklund, P. C.; Hadon, R. C. *Science* **1998**, *282*, 95.
(14) Star, D. W. Steuerman; Heath, J. R.; Stoddart, J. F. *Angew. Chem., Int. Ed.* **2002**, *41*, 2508.
(15) Mamedov, A.; Kotov, N. A.; Prato, M.; Guldi, D. M.; Wicksted, J. P.; Hirsch, A. *Nat. Mater.* **2002**, *1*, 190.
(16) Strano, M. S.; Dyke, C. A.; Usrey, M. L.; Barone, P. W.; Allen, M. J.; Shan, H.; Kittrell, C.; Hauge, R. H.; Tour, J. M.; Smalley, R. E. *Science* **2003**, *301*, 1519.

(17) Chattopadhyay, D.; Galeska, I.; Papadimitrakoulos, F. *J. Am. Chem. Soc.* **2003**, *125*, 3370.
(18) Zheng, M.; Jagota, A.; Semke, E. D.; Diner, B. A.; Mclean, R. S.; Lusting, S. R.; Richardson, R. E.; Tassi, N. G. *Nat. Mater.* **2003**, *2*, 338.
(19) Petrov, P.; Stassin, F.; Pagnoulle, C.; Jerome, R. *Chem. Commun.* **2003**, 2904.
(20) Li, H.; Zhou, B.; Lin, Y.; Gu, L.; Wang, W.; Fernando, K. A. S.; Kumar, S.; Allard, L. F.; Sun, Y.-P. *J. Am. Chem. Soc.* **2004**, *126*, 1014.
(21) Banerjee, S.; Wong, S. S. *J. Am. Chem. Soc.* **2004**, *126*, 2073.
(22) Nakashima, N.; Tomonari, Y.; Murakami, H. *Chem. Lett.* **2002**, 638.
(23) Murakami, H.; Nomura, T.; Nakashima, N. *Chem. Phys. Lett.* **2003**, *378*, 481.
(24) Nakashima, N.; Okuzono, S.; Murakami, H.; Nakai, T.; Yoshikawa, K. *Chem. Lett.* **2003**, *32*, 456.
(25) Martel, R.; Shea, H. R.; Avouris, P. *Nature* **1999**, *398*, 299.
(26) Cohen, E.; Mahadevan, L. *Proc. Natl. Acad. Sci. U.S.A.* **2003**, *100*, 12141.
(27) Zha, F.-X.; Bertsche, G.; Croitoru, M.; Kentsch, C.; Roth, S.; Kern, D. P. *Carbon* **2004**, *42*, 885.
(28) Sano, M.; Kamino, A.; Okamura, J.; Shinkai, S. *Science* **2001**, *293*, 1299.
(29) Shea, H. R.; Martel, R.; Avouris, P. *Phys. Rev. Lett.* **2000**, *84*, 4441.
(30) Watanabe, H.; Manabe, C.; Shigematsu, T.; Shimotani, K.; Shimizu, M. *Appl. Phys. Lett.* **2001**, *78*, 2928.
(31) Cuniberti, G.; Yi, J.; Porto, M. *Appl. Phys. Lett.* **2002**, *81*, 850.
(32) Terranova, M. L.; Sessa, V.; Orlanducci, S.; Rossi, M.; Manno, D.; Micocci, G. *Chem. Phys. Lett.* **2004**, *388*, 36.
(33) Gao, R.; Wang, Z. L.; Fan, S. *J. Phys. Chem. B* **2000**, *104*, 1227.
(34) Hou, H.; Jun, Z.; Weller, F.; Greiner, A. *Chem. Mater.* **2003**, *15*, 3170.
(35) Ahlskog, M.; Seynaeve, E.; Vullers, R. J. M.; Van Haesendonck, C.; Fonseca, A.; Hernadi, K.; Nagy, J. B. *Chem. Phys. Lett.* **1999**, *300*, 202.
(36) Kataura, H.; Maniwa, Y.; Kodama, T.; Kikuchi, K.; Hirahara, K.; Suenaga, K.; Iijima, S.; Suzuki, S.; Achiba, Y.; Krätschemer, W. *Synth. Met.* **2001**, *121*, 1195.
(37) Noguchi, H.; Yoshikawa, K., *J. Chem. Phys.* **1998**, *109*, 5070.
(38) Sakaue, T.; Yoshikawa, K. *J. Chem. Phys.* **2002**, *117*, 6323.
(39) Sakaue, T. *J. Chem. Phys.* **2004**, *120*, 6299.
(40) Iwataki, T.; Kidoaki, S.; Sakaue, T.; Yoshikawa, K. *J. Chem. Phys.* **2004**, *120*, 4004.
(41) Kavan, L.; Dunsch, L.; Kataura, H.; Oshiyama, A.; Otani, M.; Okada, S. *J. Phys. Chem. B* **2003**, *107*, 7666.
(42) Kataura, H.; Kumazawa, Y.; Maniwa, Y.; Umezu, I.; Suzuki, S.; Ohtsuka, Y.; Achiba, Y. *Synth. Met.* **1999**, *103*, 2555.
(43) O'Connell, M. J.; Bachilo, S. M.; Huffman, C. B.; Moore, V. C.; Strano, M. S.; Haroz, E. H.; Rialon, K. L.; Boul, P. J.; Noon, W. H.; Kittrell, C.; Ma, J.; Hauge, R. H.; Weisman R. B.; Smalley, R. E. *Science* **2002**, *297*, 593.